WIND TUNNEL SIMULATION OF SHIP-BORNE HELICOPTER OPERATIONS

PJ Skinner
Defence Aeronautics Programme, Defencetek, CSIR
pskinner@csir.co.za

Abstract

The helicopter-ship interface is simulated in a wind tunnel at a scale of ~1:10. The ship was a MEKO A-200 Frigate and the helicopter was a commercial Agusta A109 Radio Controlled model. The ship air wake was characterised by 7-hole probe scans at reduced scale. Effects of geometric approximations and atmospheric boundary layer presence were found to be significant. Results are presented for simulated helicopter-ship operations at β = 0° for a single thrust coefficient and advance ratio. Interference effects are shown for all force and moment axes of the 6-component helicopter balance. The Radio Controlled model approach was found to be useful as a research tool for research into interference aerodynamics.

Nomenclature

A = area, m^2

cref = reference chord, m

CFD = Computational Fluid Dynamics

D = rotor diameter, m

fl_w = wind axis lift force, N

fcw_w = wind axis cross wind force, N

fd_w = wind axis drag force, N

mll_w = wind axis roll moment, Nm

mlm_w = wind axis pitch moment, Nm

mln_w = wind axis yaw moment, Nm

mrc = moment reference centre

N = number of blades

ps = static pressure, Pa

R = rotor radius, m

RC = Radio Control

tpp = tip path plane

Vmag = velocity magnitude, m/s

w = vertical velocity component (downwash), positive upwards

WT = wind tunnel

α = Angle of Attack, °

β = Angle of Sideslip, °

ρ = air density, kg/m^3

ω = rotation speed, rad/s

μ = advance ratio, $V/\omega R$

C_T' = thrust coefficient, $\dfrac{fl_w}{\rho A(\omega R)^2}$

σ = solidty, $N\ cref\ /\ \pi R$

Introduction

The operating envelope of rotary wing aircraft allows for flight in close proximity to structures. In the presence of wind these structures produce wakes that disturb the local flow field for some finite distance downstream. The force multiplying effect of combining helicopters and naval vessels has seen the emergence of small vessels incorporating flight decks and hangers to support helicopter operations. Such operations force routine encounters between the helicopter and the wake of the vessel. The chaotic nature of bluff body type wakes makes it prudent to establish safe operating envelopes for the helicopter-ship combination.

Sea trials for this purpose are costly and require “cooperation” of the elements to achieve maximum benefits. Simulation of the helicopter-ship combination can serve as a useful tool to more clearly understand the interactions involved. This may serve as a guide to more effectively accomplish sea trials as well as providing training for prospective pilots. Training may only take the form of theoretical interpretation of the helicopter-wake interactions to warn the pilots of what to expect. However the scope of software simulations is reaching a maturity that allows the incorporation of influence coefficients of wakes into the simulation so that greater fidelity man-in-the-loop simulations may be performed.

It is against the backdrop of such operational support for education, training and simulation that work was started towards simulation of the helicopter-ship interface at CSIR.

Characterisation of the ship air-wake was performed by 7-hole probe measurements at reduced scale (1:100) to provide a data base of the wake for correlation with the interaction results. In addition, the effects of geometric simplifications and the presence of an atmospheric boundary layer were investigated.

The helicopter-ship interface was then simulated experimentally in a wind tunnel at ~1:10 scale using a MEKO A-200 Frigate and a Radio Controlled (RC) helicopter coupled to a 6-component balance. Time averaged loads were recorded as the helicopter was traversed in a regular pattern through the ship air-wake. The current investigation is for $\beta = 0°$.

Test Apparatus

The experiments were done in the Two Metre Wind tunnel (2mWT) and Seven Metre Wind tunnel (7mWT) (7.5mx6.5m) at CSIR, South Africa.

The 2mWT is a continuous, open jet (~1.7m diameter), open return wind tunnel and was used for the 1:100 scale ship air-wake characterisation studies. Two 1:100 scale models of the MEKO Class Frigates were built (Figure 1). One was of higher fidelity in which all the dominant features were accurately reproduced. Small scale features such as rails, antennas, etc. were excluded. The second was of greatly simplified geometry where only the basic shape of the dominant features was used. The idea was to determine whether the geometry could be relaxed for a 1:10 scale model to be used for the helicopter-ship interface studies.

The ship models were attached to a turntable located in a splitter plate across the centre of the test section to simulate the sea surface (Figure 2). To determine the effect of the atmospheric boundary layer, spires (Ref 1) were introduced at the entrance to the test section.

The 7-hole probe was supported on an arm attached to an XYZ traverse table located outside of the open jet.

For the helicopter-ship interface studies a ~1:10 scale (actual 1:9.57) model of the MEKO A-200 Frigate was built. The geometry was a compromise between higher fidelity and relaxed fidelity. The sections of the superstructure immediately upwind of the flight deck were represented accurately (up to the main mast). The bridge superstructure region was modelled only approximately. The hull was accurately modelled. The bow region was not modelled - at this scale the bow region would have extended into the wind tunnel contraction and it was decided to terminate the model at this point.

High end commercial radio controlled (RC) helicopters offer the potential of relatively low cost research tools for rotorcraft studies. Recent work on rotorcraft wakes at CSIR (Ref 2) saw the use of such RC helicopters and it was a logical extension to further exercise their potential as research vehicles into aerodynamic interaction studies

The helicopter model used was a fully articulated 46-size RC model of the Agusta A109 helicopter. The four bladed main rotor rotated in the clockwise sense when viewed from above. The blades were made from glass fibre and had a 21% cut-out and up to 94% radius had constant chord (48mm); constant thickness (~16%); and zero twist. The blade tips comprised 2-stage compound linear taper providing a rotor diameter of 1318mm.

The fully articulated main rotor had collective and cyclic control. Spherical bearings at the cuff allowed for limited flapping and the attachment hinge allowed for lead/lag motion. The 2-bladed tail rotor had collective control and lead/lag hinges. The helicopter was attached to a 6-component balance for the measurement of the forces and moments. Space constraints dictated that the balance assembly was located below the fuselage, i.e. exposed to the external flow field. A bearing arrangement along the balance longitudinal axis allowed a roll degree of freedom for the model which is necessary for trimmed flight at $\beta = 0°$. The helicopter was clamped at fixed roll angles for this test series.

The diameter of the RC model rotor determined the scale of the experimental simulation. The local Navy had ordered Super Lynx helicopter for operations with the frigates. The RC helicopter rotor was approximately 1:10 of the Super Lynx rotor. The desire was to simulate Super Lynx operations with the Agusta A109 RC helicopter. Low advance ratio operations typical of the helicopter-ship interface are dominated by rotor aerodynamics and downwash with the fuselage playing a secondary role, due to the low dynamic pressures. It was therefore felt that the fuselage assumption was justified. So a ~1:10 (actual 1:9.57) scale MEKO A-200 Frigate was built for the tests

A brushless DC electric motor was used to drive the helicopter rotor through the standard clutch assembly. Power was supplied from an external DC power supply which required significant capacitor treatment to smooth ripple. The main rotor test speed was approximately 1200 RPM yielding a tip speed of about 83 m/s and a tip Reynolds number of about 220 000.

The helicopter model was mounted to the balance assembly using rubber dampers which proved essential to eliminate ground resonance effects. The earthed part of the balance was attached to a variable pitch mechanism, which allowed for the active control required during trimmed flight for the helicopter (Figure 3).

The entire helicopter assembly was attached to a counter weighted strut extension assembly. This was fixed to the wind tunnel's integral overhead XYZϕ traverse system (Figure 4) which was used to support and position the helicopter at the required longitudinal, lateral, and vertical locations relative to the ship flight deck for the tests.

The 6-component strain gauge balance measured the aerodynamic forces on the model and the fuselage pitch and roll angles were measured by potentiometers. A computer was used to control the

RC helicopter by supplying analogue control signals to the control inputs on the radio which were transmitted to the helicopter. The standard RC receiver was used with an external power supply.

Software control loops used feedback from the balance and attitude potentiometers to drive the control hardware to achieve a trimmed flight attitude according to the arrangement in Table 1. The tethered nature of the support system meant that the attitude response had to be provided by the support system. For these tests the roll angle was fixed. The pitch motion was supplied by a motor. A motor driven yaw axis was incorporated into the support system but was these tests were all performed at $\beta = 0°$.

Table 1: Helicopter control architecture

Helicopter channel	**Feedback signal**
Main rotor collective	Net lift force
Tail rotor collective	Net yaw moment about mrc
Longitudinal cyclic	Net drag force
Roll angle	Net side force
Lateral cyclic	Roll angle
Pitch angle	Net pitch moment about mrc
Throttle	Main rotor RPM

The origin of the coordinate system was the centre of a circle through the port edge, starboard edge and he the aft most point of the flight deck. From this origin, x is positive forward, y is positive to starboard, z is positive upwards. The traverse path that the model helicopter followed is indicated in Figure 5.

The three force and three moment coefficients available from the 6-component strain gauge balance were recorded in these tests (convention when looking upwind from behind the helicopter):

$$C_D = \frac{fd_w}{\rho A(\omega R)^2}\text{; + downwind}$$

$$C_Y = \frac{fcw_w}{\rho A(\omega R)^2}\text{; + to starboard}$$

$$C_T' = \frac{fl_w}{\rho A(\omega R)^2} \approx C_T\text{; + up}$$

$$C_l = \frac{mll_w}{\rho A(\omega R)^2 R}\text{; + starboard side down}$$

$$C_m = \frac{mlm_w}{\rho A(\omega R)^2 R}\text{; + nose up}$$

$$C_n = \frac{mln_w}{\rho A(\omega R)^2 R}\text{; + nose to starboard}$$

A pseudo thrust coefficient was used which is based on the net lift force in the wind axis system. The typically small variations in the tip path plane from the horizontal meant that this was a reasonable approximation of C_T.

The forces and moments refer to net loads, i.e. the effects of model mass have been removed and the moments have been transferred to the required mrc for the helicopter.

Test Procedure

The helicopter was started and brought to a hover condition using a combination of manual and automatic control. The wind tunnel was then started and accelerated to speed while the control loops trimmed the helicopter. When the conditions were satisfactorily stable the attitude and control surfaces were locked for the traverse tests.

The "trim" exercise was performed off to the side of the ship but due to the confines of the tunnel the helicopter was probably not in free conditions. The helicopter roll axis was not driven and this was fixed at an estimated trimmed roll angle prior to the tests. Offsets in the data, particularly in the roll moment, should be expected.

The test conditions are presented in Table 2.

Table 2 Test conditions

C_T'/σ	~0.047
μ	~0.076
RPM	1200

Test Results

Flow field measurements

Sample results from the 7-hole probe measurements are shown in Figures 6 to 8. The mean longitudinal velocity gradients in Figure 6 are seen to be small. The 7-hole probe cannot measure reverse flow and there is reverse flow present in the separation zone immediately downwind from the hangar. However the flow has reattached for the region scanned by the 7-hole probe (confirmed by flow visualisation) and therefore the results are meaningful. Figure 6 also indicates the measurable differences in the wake produced by the relaxed fidelity model. These were relatively small for $\beta = 0°$, but became unacceptably large as sideslip was introduced. Therefore relaxing fidelity requirements for wake modelling should be approached with caution. Of course distance from the wake source to the point of interest is significant but certainly for near wake studies such as this, with the close proximity of the helicopter hangar, it is necessary to model the hangar realistically for an accurate wake. The significance of accuracy is not clear however,

particularly in the light of idealised environment with no pitch and roll motion of the deck.

The velocity gradients in the lateral plane are more significant (Figure 7). The effects of the spires (velocity profile) and relaxed fidelity model on the wake are shown in greater detail in Figure 8. The position corresponds to the lowest lateral scan along the y-axis in the helicopter traverse tests. The relaxed fidelity model produced steeper angles in the wake and increased the wake dimensions. This should not be surprising considering the extreme bluntness of the model. The effect of the spires was small on the angularity but significant on the velocity. This is to be expected as one of the primary functions of spires is to reduce the velocity near to the surface, i.e. produce a velocity gradient. The spires were located too close to the model due to the short test section size and the individual wakes are clear in the data at lateral intervals of 200 mm which was the spire spacing used. This was responsible for the apparent deviations in flow angle in Figure 8a but the mean flow angle tracks the result without spires reasonably well. Note that the spire turbulence scales were not considered.

The significant flow features of the wake in terms of helicopter operations are a downwards tilt to the velocity vector and a reduction in its magnitude. Both of these effects will produce a reduction in lift from the helicopter rotor. This will affect the rotor helicopter moments due to the 90° phase lag inherent in the rotor dynamics.

There is a slight asymmetry in Figure 7 which is produced by the cut-out in the starboard side of the hangar structure immediately upwind of the flight deck (Figure 2).

In the 7mWT, used for the larger scale simulations, there was even less fetch distance for the spires and they were not included in the simulation. In reality then, the effect of the ship air-wake on a helicopter will be worse than indicated in the present study. The degree to which this is the case is dependent on the velocity profile. It must be stressed that this is not simply the velocity profile typically simulated over representative terrain categories but rather the superposition of such profiles and the speed of the ship.

Helicopter-traverse tests

Initially, two test types were performed; statically sampled data for which the helicopter model was stationary at each point during data acquisition and the interference was given by the mean of the number of samples at that point; dynamically sampled data for which the helicopter model was moved at a constant rate along a predefined path during data acquisition and the interference was determined from a curve fit of the data set.

The reliability of the measured data may be assessed through repeatability scans and these are shown in Figure 9 for the two test types. Both test types yielded results of acceptable quality to be used to quantify the helicopter-ship interface for this application. A comparison of the measurements from the two techniques is given in Figure 10. The source data from which the dynamic fitted data was determined has been included. This clearly shows the severe turbulence in the ship wake which produced the amplitude fluctuations in the measured data behind the superstructure. The dynamically sampled data approach offered benefits in terms of reduced test time and potentially better resolution, due to reduced discetisation error, and this approach was used for the current tests. The lateral traversing speed used for the final interference tests was approximately 40 mm/s.

The effect of the ship air-wake on the static aerodynamic coefficients of the helicopter is shown in Figure 11 for a horizontal (x-y) plane 700 mm (~0.5D) above the surface of the flight deck. Graphs from each of the components of the 6-component balance are shown. All of the components may be seen to be affected by the wake. The traverse scans did not span the same geometric range and the coordinate scales of the plots are deliberate to avoid distortion.

The open return configuration and low contraction ratio for the 7mWT make it susceptible to ambient wind fluctuations and temperature changes. Therefore the trim settings initially appropriate at the start of a scan may not be appropriate throughout the scan as the ambient conditions change. The current results should therefore be interpreted more from a change perspective rather than from absolute values. The interaction results are difficult to interpret by inspection alone, even under ideal test conditions, due to the many factors involved such as the effect of the rotor downwash, ground effect from the flight deck, asymmetrical disc loading, etc.

The thrust coefficient is showing the expected reduction over the flight deck due to the reduced magnitude of velocity and a downwards tilt of the velocity vectors. The interference pattern is essentially symmetrical. The asymmetries reported in Ref 3 have been avoided due to the use of a model with cyclic rotor control inputs.

Lateral variations across the rotor disc may be expected to produce changes about the pitch axis of the helicopter due to the 90 phase lag of the rotor dynamics and resultant tilt of the tip path plane caused by the flapping blades. Similarly, longitudinal variations across the rotor disc may be expected to produce changes about the roll axis of the helicopter. From the 7-hole probe flow field scans (Figures 6 and 7) it is clear that the gradients that exist lie in combination planes as the air flows over and around the ship. The helicopter response to the air wake should be expected to show some degree of coupling between the pitch and roll axes.

For the current rotor direction sense (clockwise from above) a downwash on the port side of the disc will produce a downwards flap of the rotor blades with a corresponding negative change in pitch moment. Applying this to the current measurements, a reduced pitch moment should exist on the starboard side of the flight deck and an increased pitch moment should exist on the port side of the flight deck. Figure 11b does indicate reduce pitch moment on the starboard side and increased pitch moment on the port side of the flight deck, but the local maxima are separated significantly in the longitudinal (x) direction.

From the 7-hole probe measurements the longitudinal gradients increased with increasing x distance (i.e. as the hangar is approached from the rear).Therefore a local maximum in the roll moment data would be expected at the closest point to the hangar. The downwash over the hangar produced a non-uniform inflow over the rotor disc which for the current rotor would have caused blade flapping to starboard with an associated positive change in roll moment. This is borne out in Figure 11e. The reason for the two zones of reduced roll moment on either side of the flight deck (beyond the deck), however, is not immediately clear.

Changes in roll moment produced by changes in the tip path plane may be expected to show corresponding changes in side force. This, correlation, however, was not detected in the measurements (Figure 11c).

The drag coefficient is reduced as expected in the ship air-wake due to the reduced wind speed (Figure 11f)

The interference shown in Figure 11 was generally reflected at all traverse heights, but with decreasing amplitude. An example of the change in interference with height is shown in Figure 12 for C_l. The two negative roll moment zones found at Z=700mm gradually disappear as the height is increased.

The interference measured in the y-z plane at x=0mm is shown in Figure 13, and that measured in the x-z plane at y=0mm is shown In Figure 14. This data serves to indicate expected load variations for flight in orthogonal approach planes to the landing point. As expected, the lateral gradients are greater than the vertical gradients which highlight potential difficulties in transition flight from open water to over the flight deck. Clearly this should be done at as great a height as possible/feasible to reduce the interference.

There is a significant difference in the symmetry of the pitch moment plot of Figure 13 (13b). The lateral gradients are significantly less (almost flat) for approaches from the port side than from the starboard side. This is probably a result of the small asymmetry in the wake geometry (Figure 7) coupled with the direction of rotation of the main rotor.

A comparison should be made with the roll moment plot of Figure 14 (14e) for the equivalent interference to be expected for approaches from aft. (Note that only a subset of the wide range in lateral scan distances in Figure 13 applies.) Changes in the pitch plane are expected, due to the event of crossing the flight deck that should produce roll moment changes in the helicopter loads as a result of the phase lag of rotor dynamics. These are seen to be rather small, and are probably related to the angle of the wake for this advance ratio. For a sufficiently flat wake angle, the presence of the flight deck would not be expected to have a significant aerodynamic influence on the rotor. There would appear to be a case for approaches from aft for this test configuration.

Conclusions

7-hole probe flow field measurements performed at 1:100 scale showed that relaxing fidelity requirements of physical models required for wake modelling should be approached with caution. For the helicopter-ship interface case, at the least the superstructure immediately forward of the flight deck should be modelled accurately.

Helicopter-ship interaction measurements were performed at β = 0° for a single thrust coefficient and advance ratio at ~1:10 scale. The ship air-wake produced clear interference trends on the helicopter static aerodynamic coefficients that were evident in the test data.

All force (3) and moment (3) axes were affected. The effect of the phase lag in the rotor dynamics was noticed although the complexity of the interaction problem precluded simple explanation of the interference based on inspection alone.

There would appear to be a case for an aft approach rather than from port or starboard for the current configuration.

References

[1] Irwin, H.P.A.H., “The Design of Spires for Wind Simulation”, Journal of Wind Engineering and Industrial Aerodynamics, Vol. 7, 1981, pp361-366.

[2] Denton, T.J., Martins, J.C.F., Ratner, G.R., and Skinner, P.J., “Experimental Characterisation and Comparison of a Model Helicopter Rotor Tip Vortex and Fixed Wing Tip Vortex”, 29th European Rotorcraft Forum, Germany

[3] Zan, S.J., “Experimental Determination of Rotor Thrust in a Ship Air wake”, American Helicopter Society Journal, April 2002

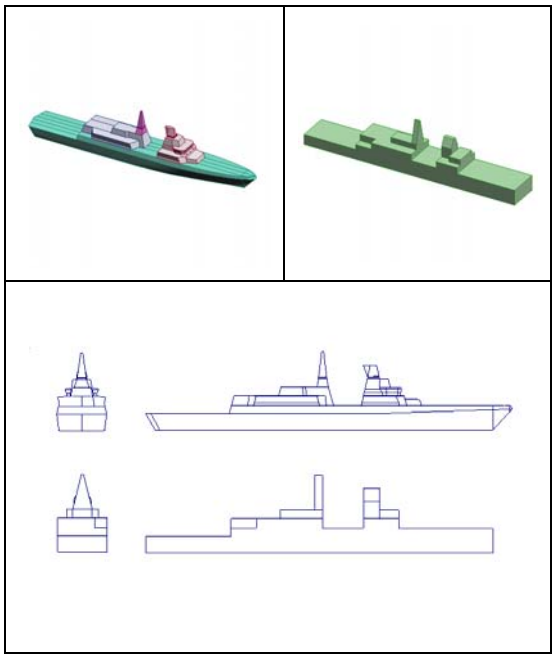

Figure 1 Higher fidelity and relaxed fidelity model of the MEKO A-200 Class Frigate

Figure 2 Higher fidelity 1:100 MEKO Class Frigate in 2mWT for flow field characterisation

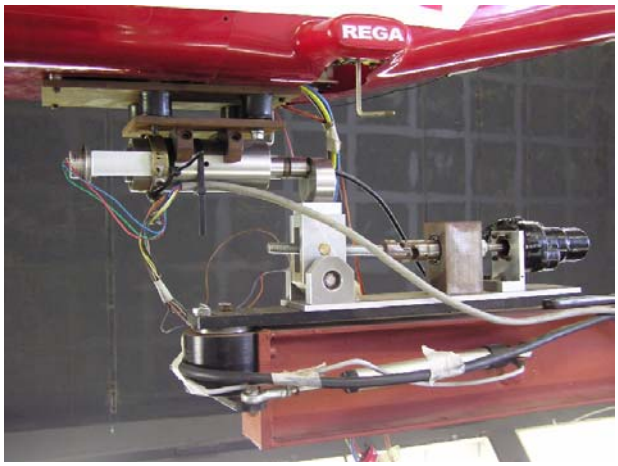

Figure 3 RC helicopter support system

Figure 4 Wind tunnel setup of ~1:10 scale helicopter-ship interface

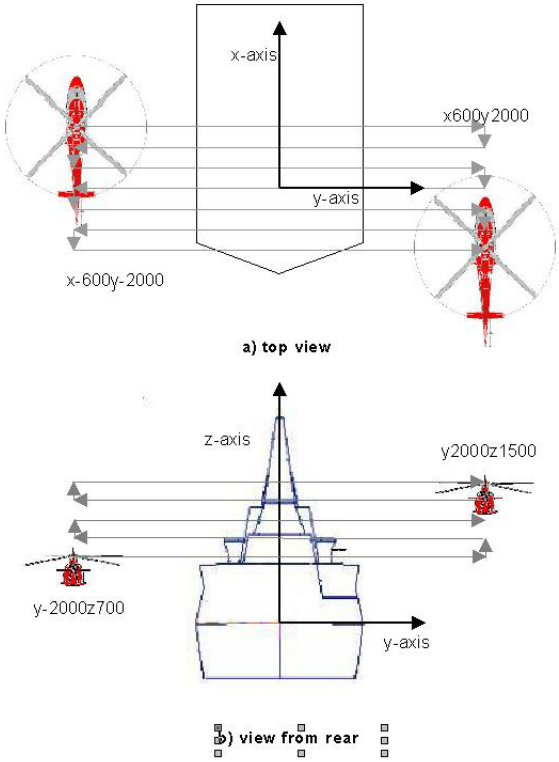

Figure 5 Traverse path over flight deck

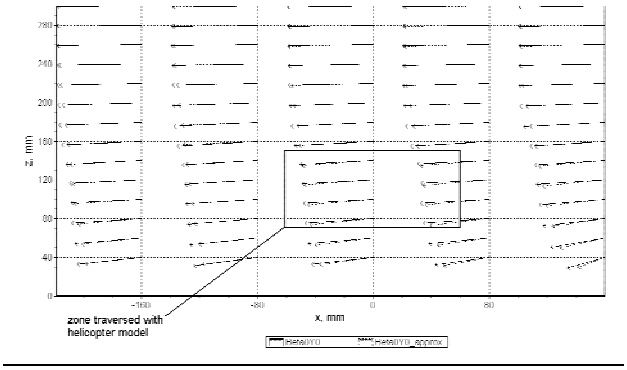

Figure 6 Velocity vectors along centre-line of flight deck for higher fidelity and relaxed fidelity (approx) models

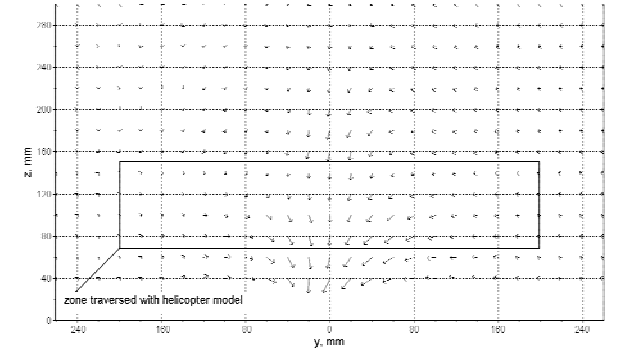

Figure 7 Velocity vectors perpendicular to the centre-line of the flight deck

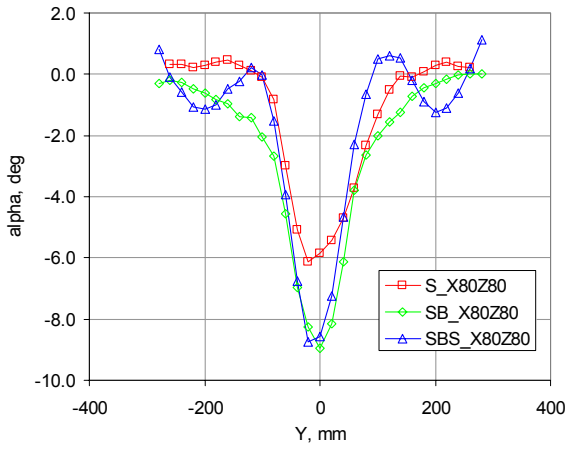

a) alpha

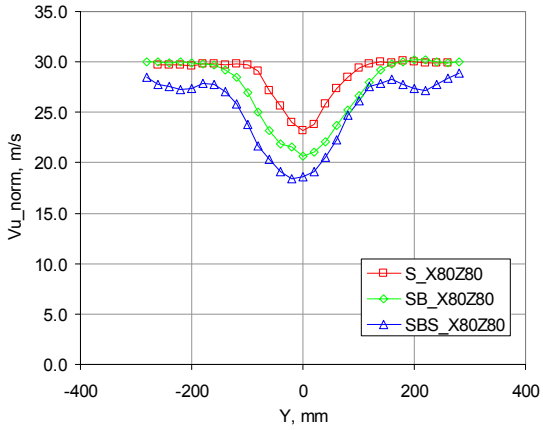

b) normalised free stream velocity component

Figure 8 Effect of spires and relaxed fidelity model on wake structure (S=higher fidelity ship; SB=relaxed fidelity ship; SBS=SB with spires)

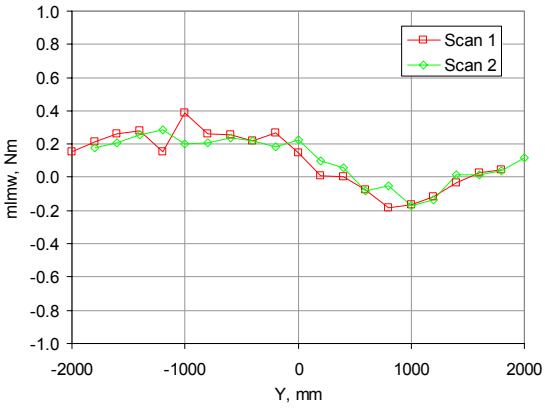

a) Statically sampled data

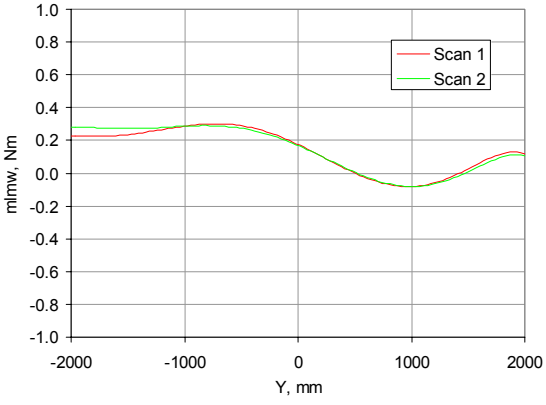

b) Dynamically sampled data

Figure 9 Repeatability of measured interference data

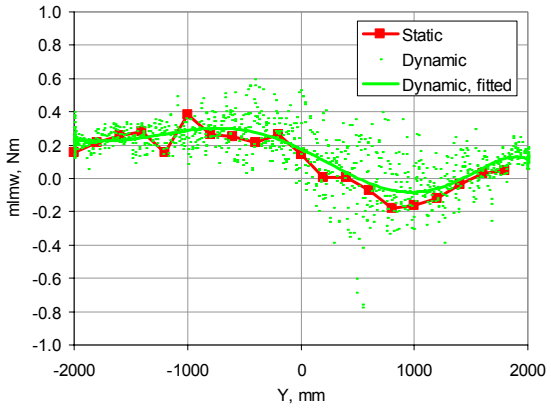

Figure 10 Comparison of statically and dynamically sampled data

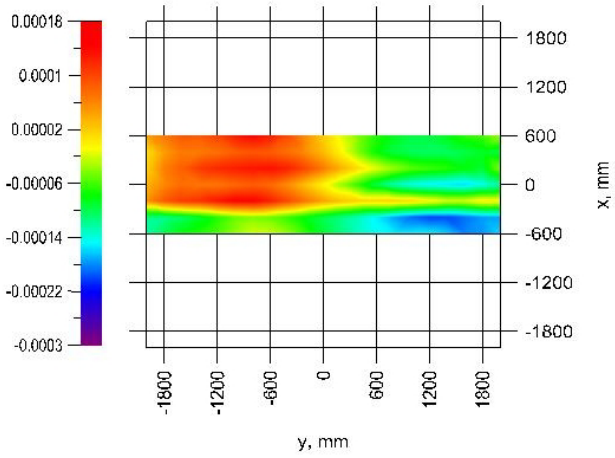

c) C_Y

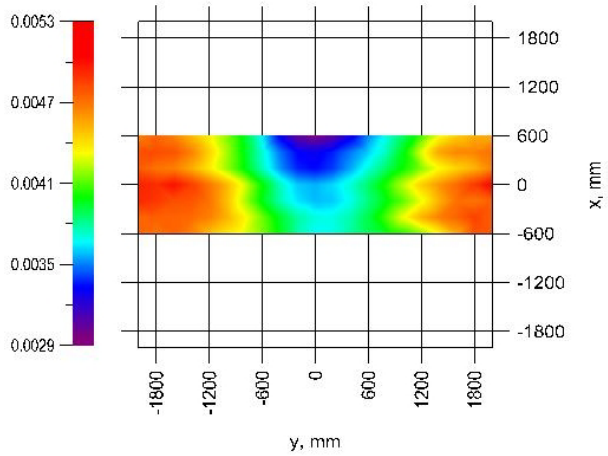

a) C_T'

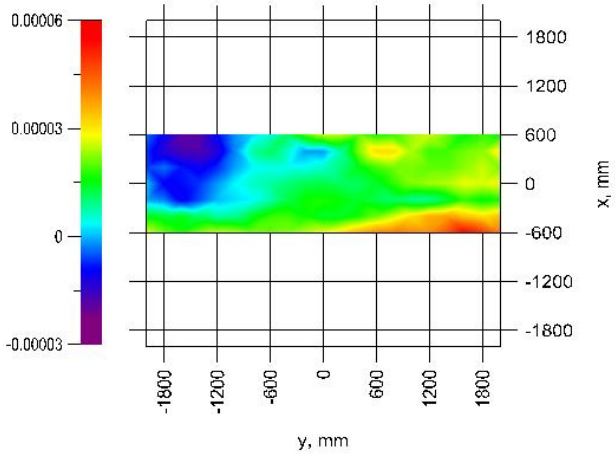

d) C_n

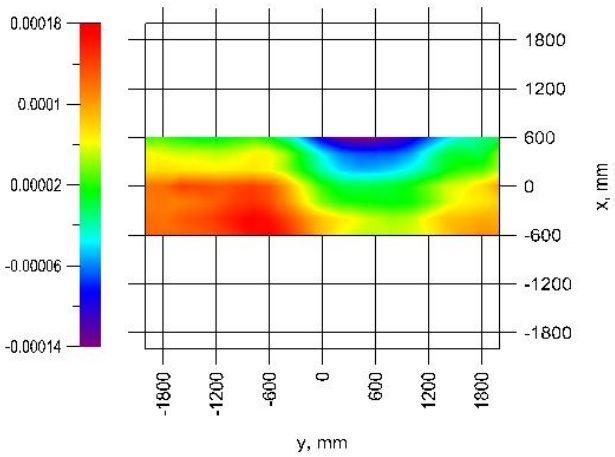

b) C_m

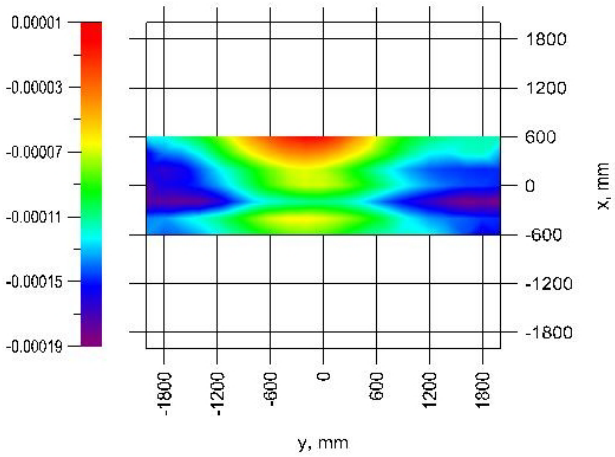

e) C_l

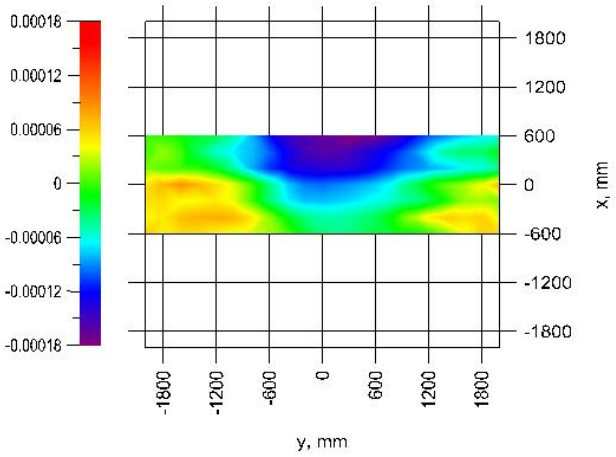

f) C_D

Figure 11 Effect of ship air-wake on helicopter static aerodynamic coefficients at C_T/σ = ~0.047; μ = 0.076; Z = 700mm (~0.5D);

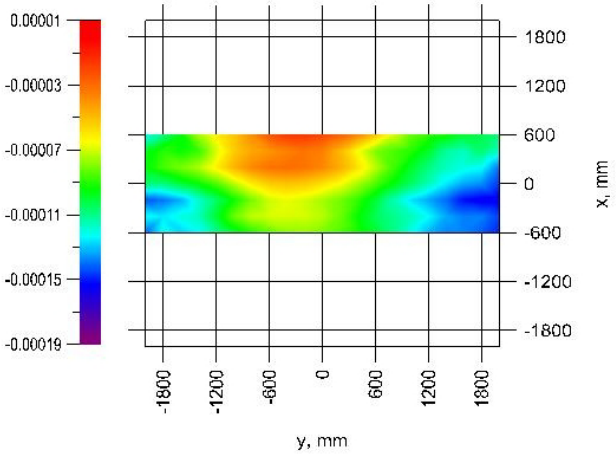

a) C_l; Z = 900mm

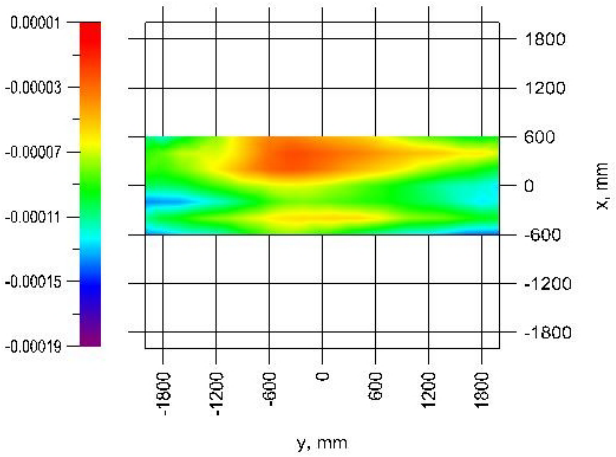

b) C_l; Z = 1100mm

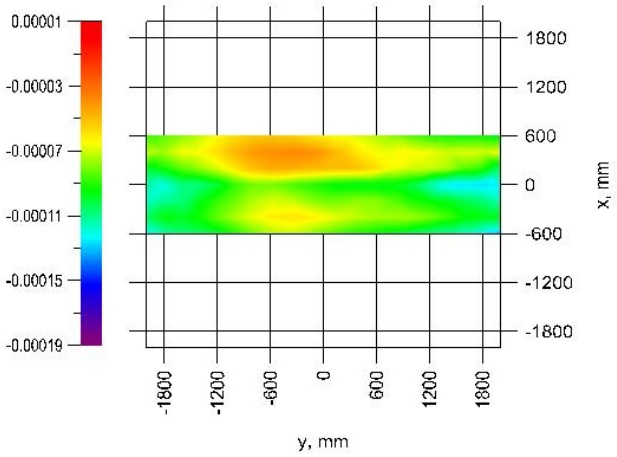

c) C_l; Z = 1300mm (~1D)

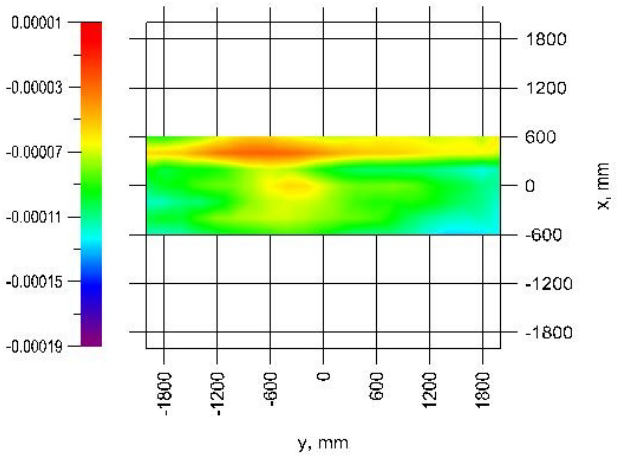

d) C_l; Z = 1500mm

Figure 12 Change in C_l with increasing height above the flight deck; C_T/σ = ~0.047; μ = 0.076

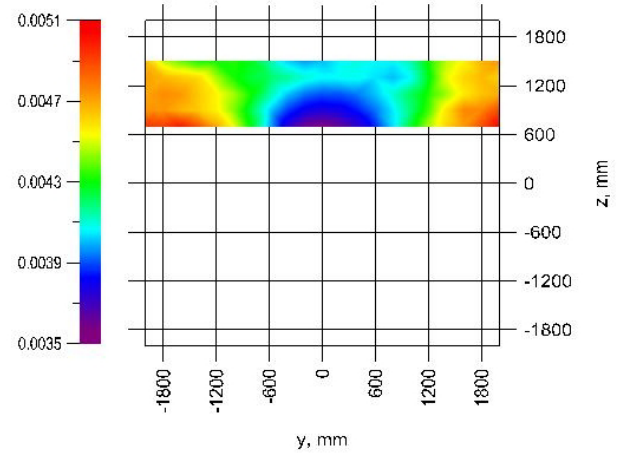

a) C_T'

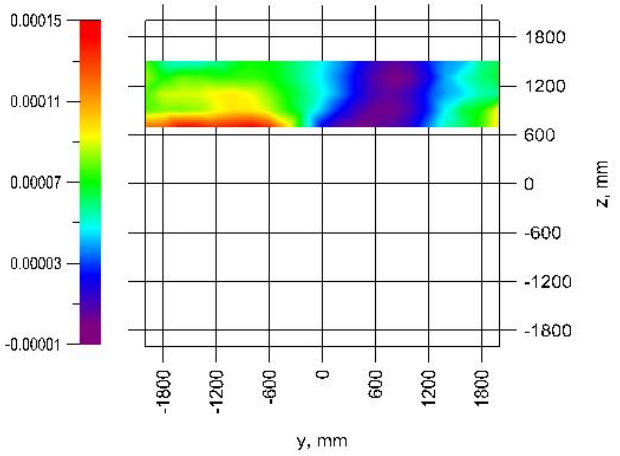

b) C_m

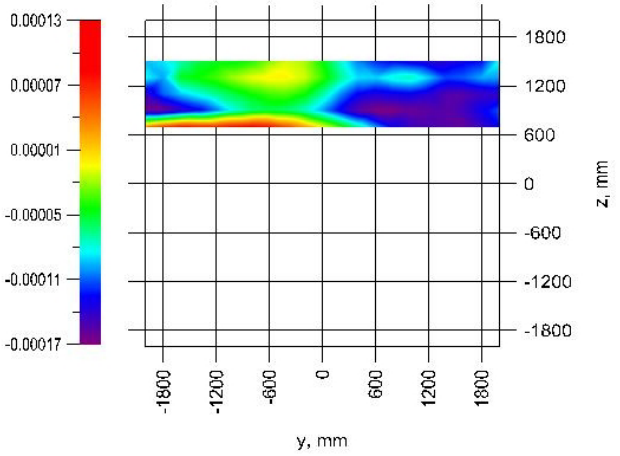

c) C_Y

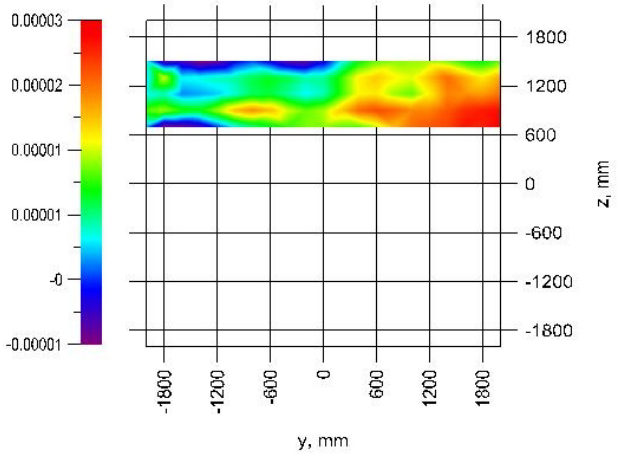

d) C_n

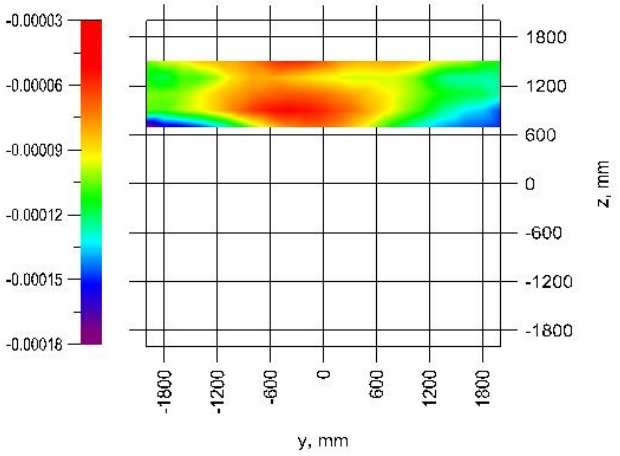

e) C_l

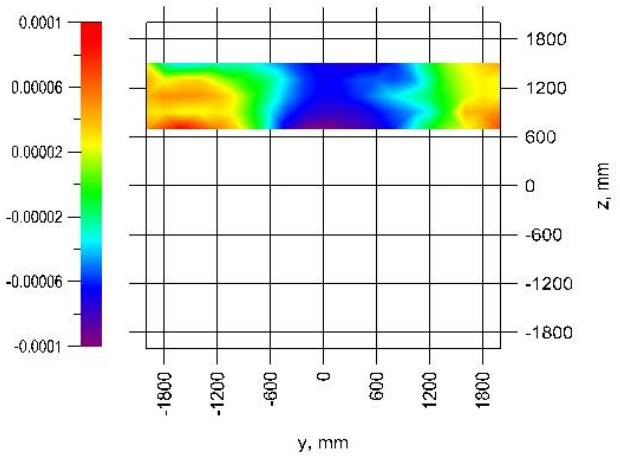

f) C_D

Figure 13 Effect of ship air-wake on helicopter static aerodynamic coefficients at C_T/σ = ~0.047; μ = 0.076; X = 0mm

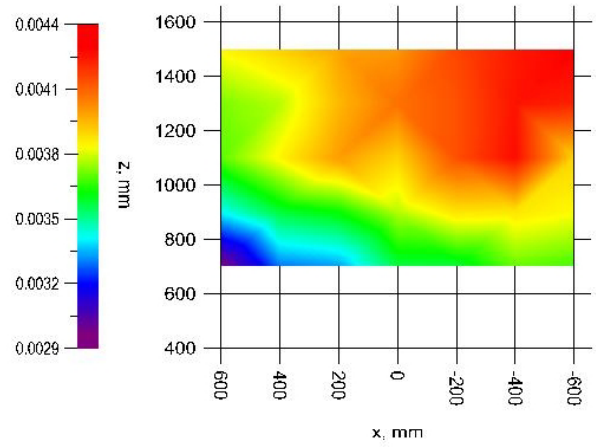

a) C_T'

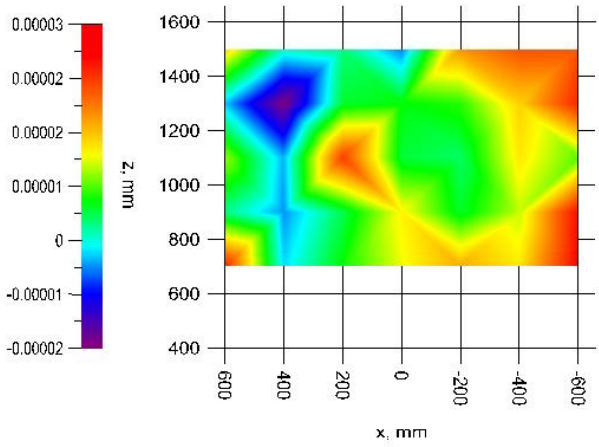

d) C_n

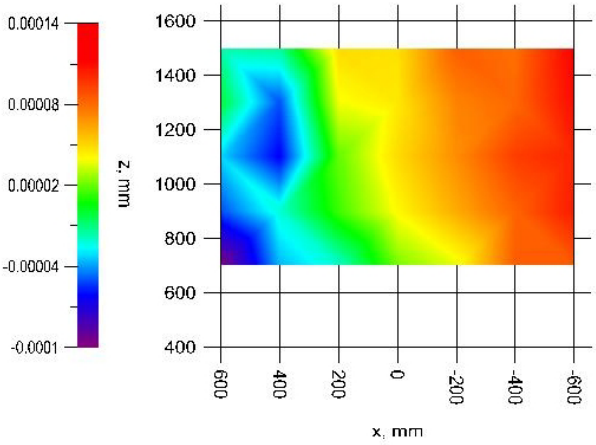

b) C_m

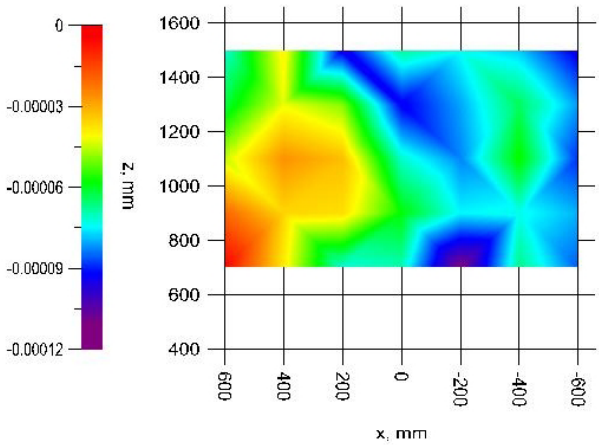

e) C_l

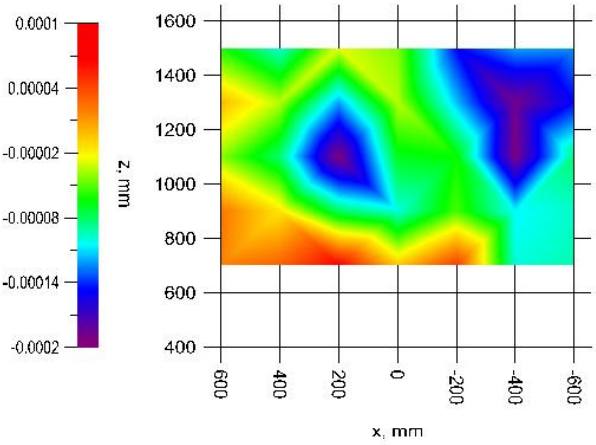

c) C_Y

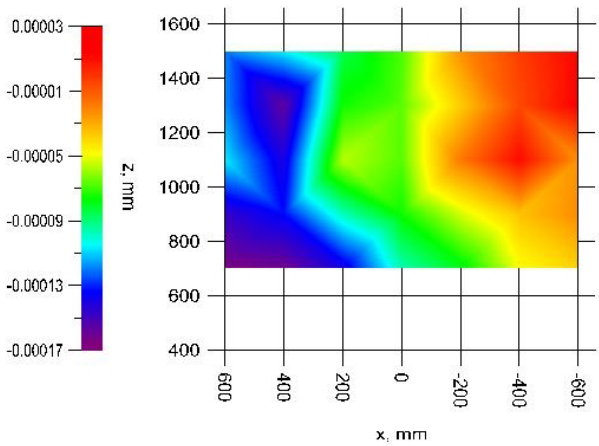

f) C_D

Figure 14 Effect of ship air-wake on helicopter static aerodynamic coefficients at C_T/σ = ~0.047; μ = 0.076; Y = 0mm